Supplementary Information (SI) for Environmental Science: Nano.

Hematite-based photoanodes decorated with oxygen-deficient CeO_2 for photoelectrocatalytic degradation of tetracycline: Pulse deposition strategy

Meiying Jia[a], Yuanyuan Ma[c], Wenxuan Wang[b], Anqi Kang[b], Ping Wang[a] *, Haiyin Xu[a], Weiping Xiong[b], Zhaohui Yang[b]

[a] Yuelushan Laboratory, College of Life and Environmental Sciences, Central South University of Forestry and Technology, Changsha 410004, P.R. China;

[b] College of Environmental Science and Engineering, Hunan University, Changsha 410082, P.R. China;

[c] State key laboratory of pollution control and Resource reuse, School of Environmental Science and Engineering, Tongji University, Shanghai 200092, P.R. China.

* Corresponding author at: College of Environmental Science and Engineering, Central South University of Forestry and Technology, Changsha, Hunan 410004, China.

Phone & Fax: +86-0731-8562-3372

E-mail address: pingwang@csuft.edu.cn

Reagents

Cerous nitrate hexahydrate ($Ce(NO_3)_3$•$6H_2O$, 99.7%), Ferrous sulfate heptahydrate ($FeSO_4$•$7H_2O$, 99.7%), Anhydrous sodium sulfate (Na_2SO_4, 99.7%), Potassium chloride (KCl, 99.7%), hydrochloric acid (HCl, 99.7%), sodium hydroxide (NaOH, 99.7%), acetonitrile (ACN, 99.7%), methanoic acid (FA, 99.7%), tert-butanol (TBA, 99.7%), sodium azide (NaN_3), Ethylenediaminetetraacetic acid disodium salt (EDTA-2Na) acetone, anhydrous ethanol were provided by Sino pharm Chemical Reagent Co., Ltd. Tetracycline (TC, 99%) was purchased from Shanghai Rhawn Technology Development Co. Ltd. Without special statement, deionized water with the specific resistance of 18.25 MΩ·cm was applied to prepare solutions. The above reagents are commercially available analytical pure and were directly used without further purification.

The photoelectrocatalytic degradation experiment

For each photoelectrocatalytic degradation experiment, the performance was assessed by the degradation of tetracycline (TC, 20 $mg \cdot L^{-1}$) in a three-electrode quartz cell (100 mL) with Na_2SO_4 as the electrolyte. After the adsorption-desorption equilibrium of TC was reached in the dark for 30 min, a light source was set at a certain distance from the photoanode for photoelectrocatalytic degradation. At each sampling time point, the solution was extracted with a syringe and 1.5 mL samples were collected with a 0.45 μm microporous filter for high performance liquid chromatography (HPLC) analysis. The intermediates of TC and the leaching concentrations of metal ions in treated water were detected by liquid chromatography-mass spectrometry (LC-MS) and ICP-MS, respectively.The specific HPLC and LC-MS analysis operation was displayed in detail as follows.

HPLC analysis operation:

The samples were filtered with 0.45 μm cellulose acetate syringe membrane filter to determine the TC concentration via (HPLC, Agilent 1100 series, USA) with an Agilent TC-C18 column (4.6 × 250 mm, 5 um). The mobile phase was a mixture of 80% oxalic acid and 20% acetonitrile. Notably, the mobile phase was sonicated for 15 min before use to remove air bubbles. The detector wavelength was set at 354 nm, and the column temperature was 30°C. Meanwhile, the flow rate and injection volumes were 0.5 mL/min and 20 μL, respectively. The retention time of TC was 3.8 min.

Liquid chromatography-mass spectrometry

Determination of the photo-electrodegradation intermediates of TC were carried out on a LC-MS system equipped with a 6460 HPLC (Agilent, USA) and an API 3000 mass analyzer. The HPLC column was a Kromasil C18 column (4.6 × 100 mm) from Agilent. 0.1% of formic acid aqueous solution and acetonitrile were used as mobile phases A and B, respectively. The eluent flow rate keeps 0.45 mL/min. An injection volume of 10 μL was used in analysis and column temperature at 302 K (30°C). Linear gradient elution as follows: The gradient solvent was as followed: A=90% (0 min), 10% (10 min), 10% (14 min), 90% (15 min), 90% (16 min). Max pressure limit: 1300 bar.

Characterization

The surface morphology and structure of the catalyst were recorded by emission scanning electron microscopy (FE-SEM). X-ray diffractometer (XRD) analysis was performed using Bruker D8 (scanning Angle:5-90°). X-ray photoelectron spectroscopy (XPS) was performed on Thermo ESCALAB 250XI instrument using an Al-k-α X-ray source to characterize the chemical composition and valence states of the catalyst materials. Fourier transform infrared spectroscopy (FTIR) was obtained using a Fourier transform infrared spectrometer (NICOLET iS10) in the range of 4000-400 cm^{-1}. The UV-vis absorption (DRS) spectra and photoluminescence (PL) spectra were detected by Varian Cary 300 spectrophotometer and PerkinElmer LS-55 fluorescence, respectively. Electron paramagnetic resonance (EPR) signals were detected with the Bruker A300 spectrometer. The mineralization of TC was estimated by total organic carbon (TOC) using Shimadzu TOC-VCPH analyzer.

The photoelectrochemical performance test

An electrochemical station (CHI 660E, Shanghai Chenhua) was used for photoelectrochemical measurements in Na_2SO_4 electrolyte. The FTO-α-Fe_2O_3@CeO_2 photoanode was used as the working electrode, and the Ag/AgCl electrode and the Pt sheet were used as the reference and counter electrodes, respectively. The measured potential versus Ag/AgCl was converted to a standard hydrogen electrode (NHE) by $E_{NHE} = E_{Ag/AgCl} + 0.197$. The visible light source was a PLS-SXE 300 W xenon lamp equipped with a cut-off filter to ensure visibility ($\lambda > 420$ nm), and the optical density parameter was 0.318 $W\cdot cm^{-2}$.

$$i = i_0\left[exp\left(\frac{\alpha_a nFE}{RT}\right) + exp\left(\frac{\alpha_c nFE}{RT}\right)\right] \quad (1)$$

where i represents the current density; i0 represents the exchange current density; α_a represents the anodic electron transfer coefficient; α_c represents the cathodic electron transfer coefficient; n represents the number of electrons transferred in the reaction; F represents Faraday's constant; E represents the applied voltage; R represents the universal gas constant, T represents the thermodynamic temperature.

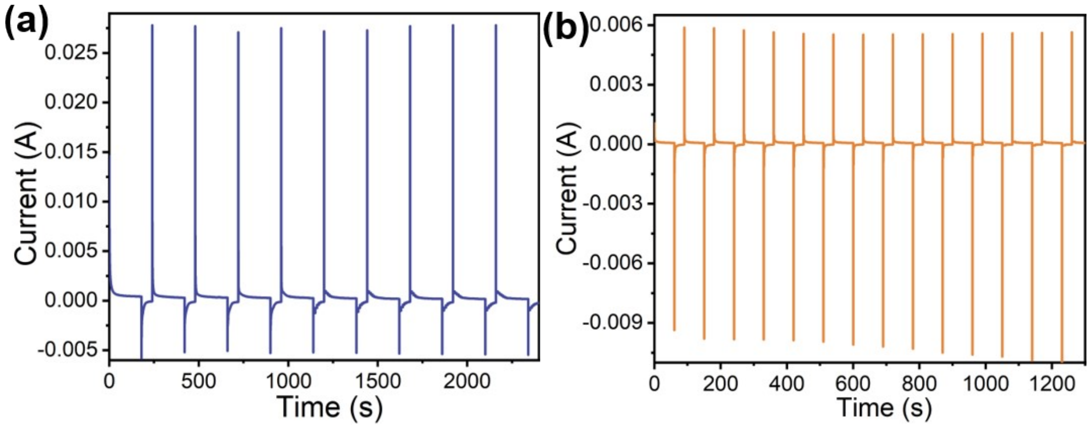

Fig. S1 Pulse deposition current-time curve of (a) FTO-α-Fe_2O_3 photoanode, (b) FTO-CeO_2 photoanode.

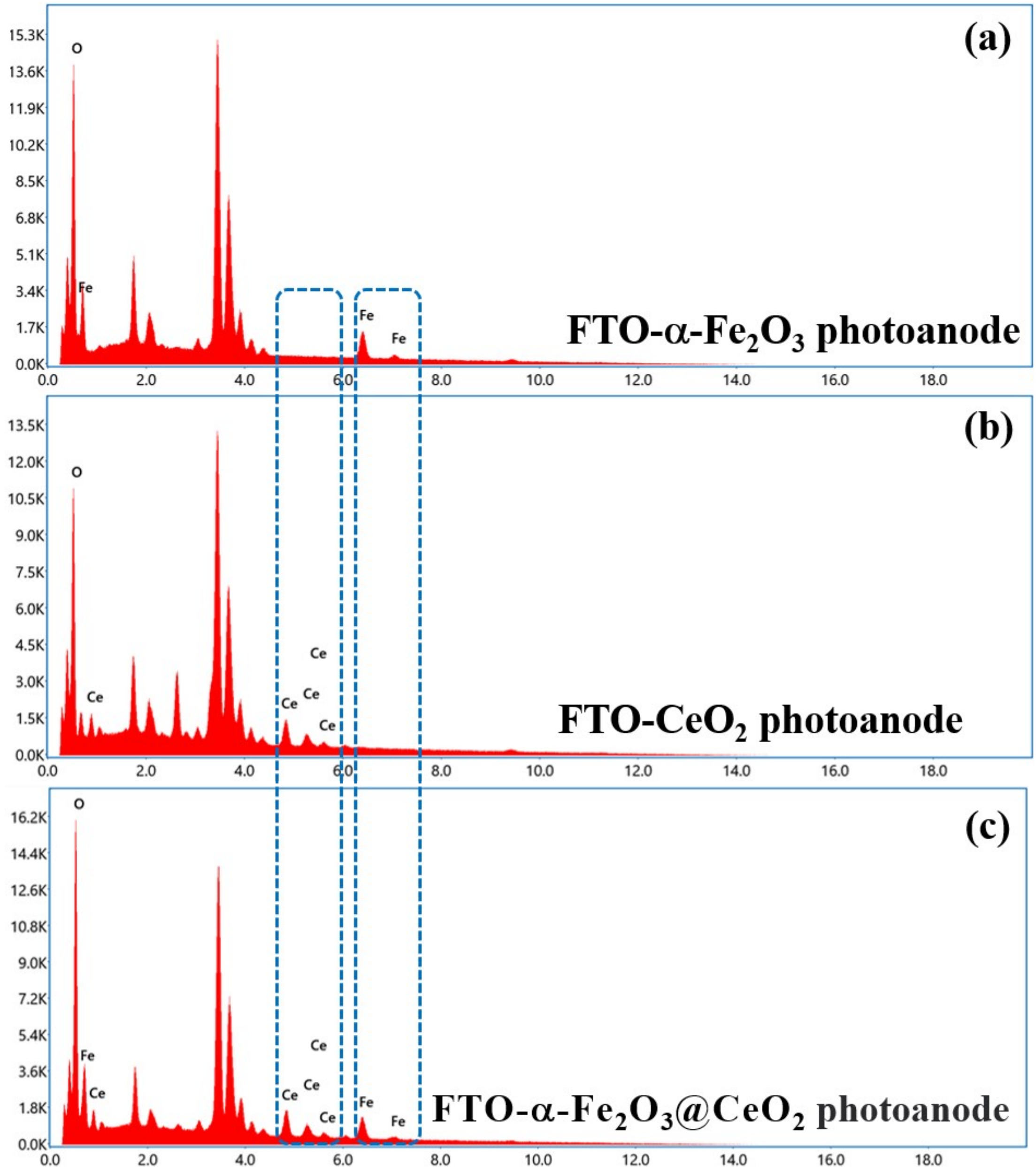

Fig. S2 SEM-EDS spectrum of FTO-α-Fe$_2$O$_3$ photoanode, FTO-CeO$_2$ photoanode, and FTO-α-Fe$_2$O$_3$@CeO$_2$ photoanode.

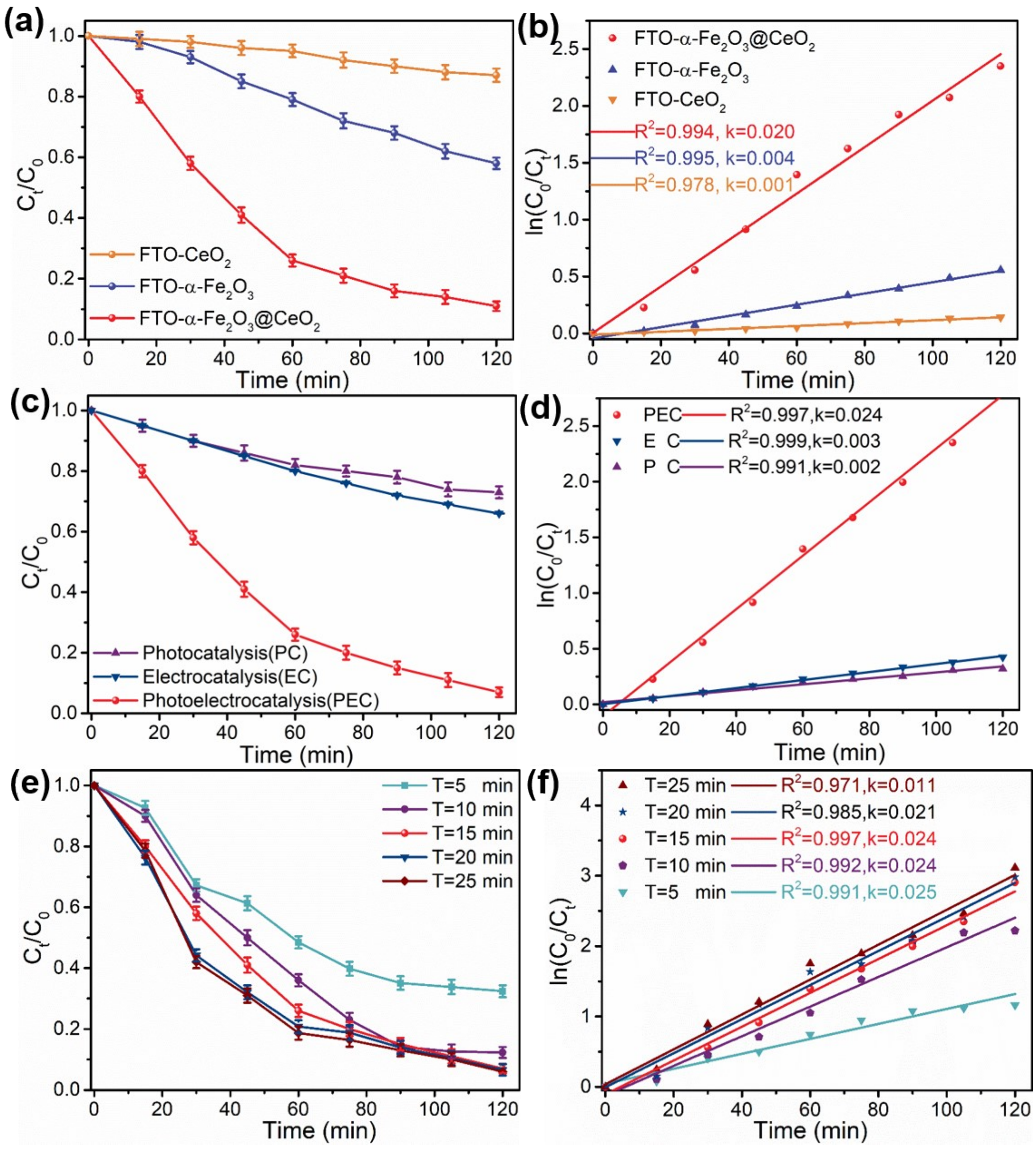

Fig. S3 (a) Degradation dynamics and (b) pseudo-first-order kinetic curves of TC using different photoanodes; (c) comparison of TC degradation dynamics and (d) pseudo-first-order kinetic curves using FTO-α-Fe_2O_3@CeO_2 photoanode under different processes. Effect of (e) deposition time on the PEC degradation and (f) degradation dynamics.

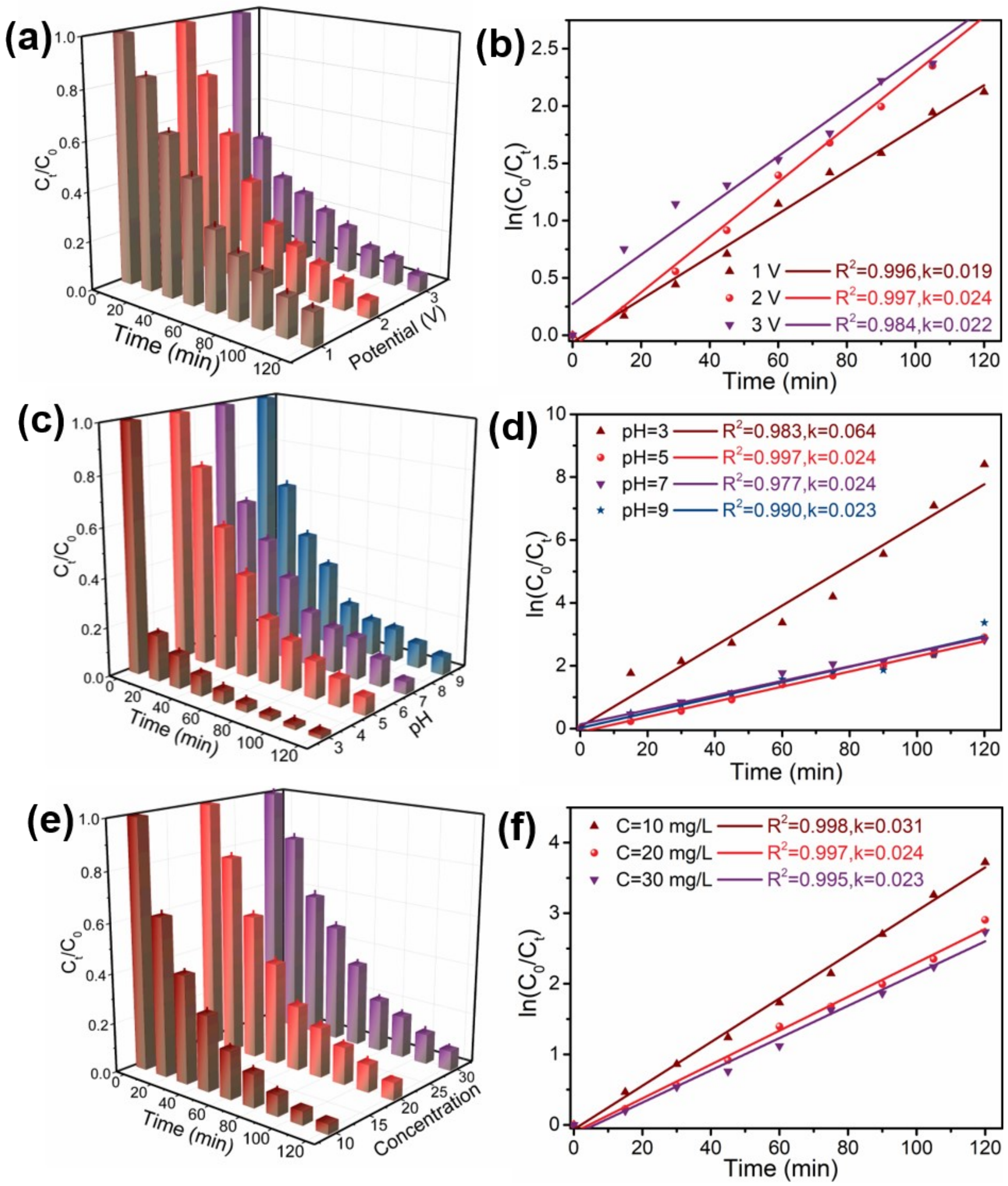

Fig. S4 Effect of (a) external potential on the PEC degradation and (b) degradation dynamics; Effect of (c) pH on the PEC degradation and (d) degradation dynamics; (e) Effect of antibiotic concentration and (f) degradation dynamics.

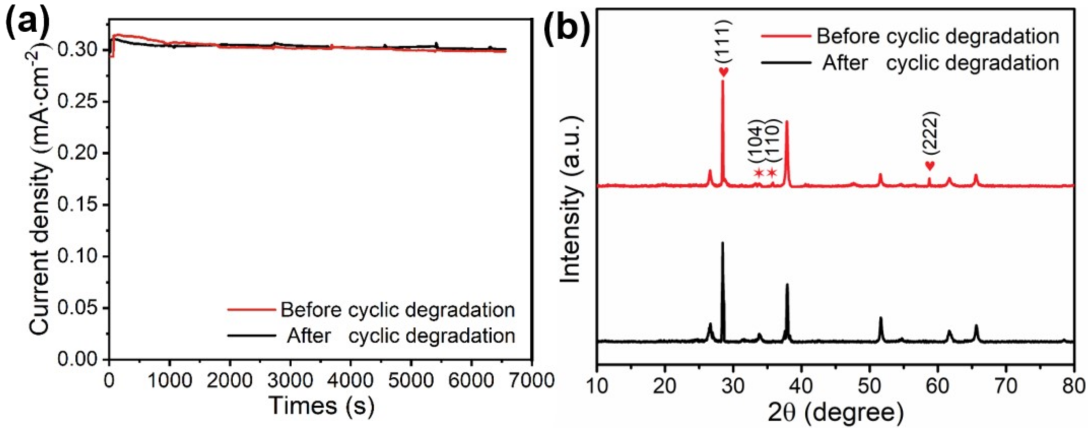

Fig. S5 (a) Long-time photocurrent decay curve; (b) XRD patterns of FTO-α-Fe_2O_3@CeO_2 before and after cyclic degradation.

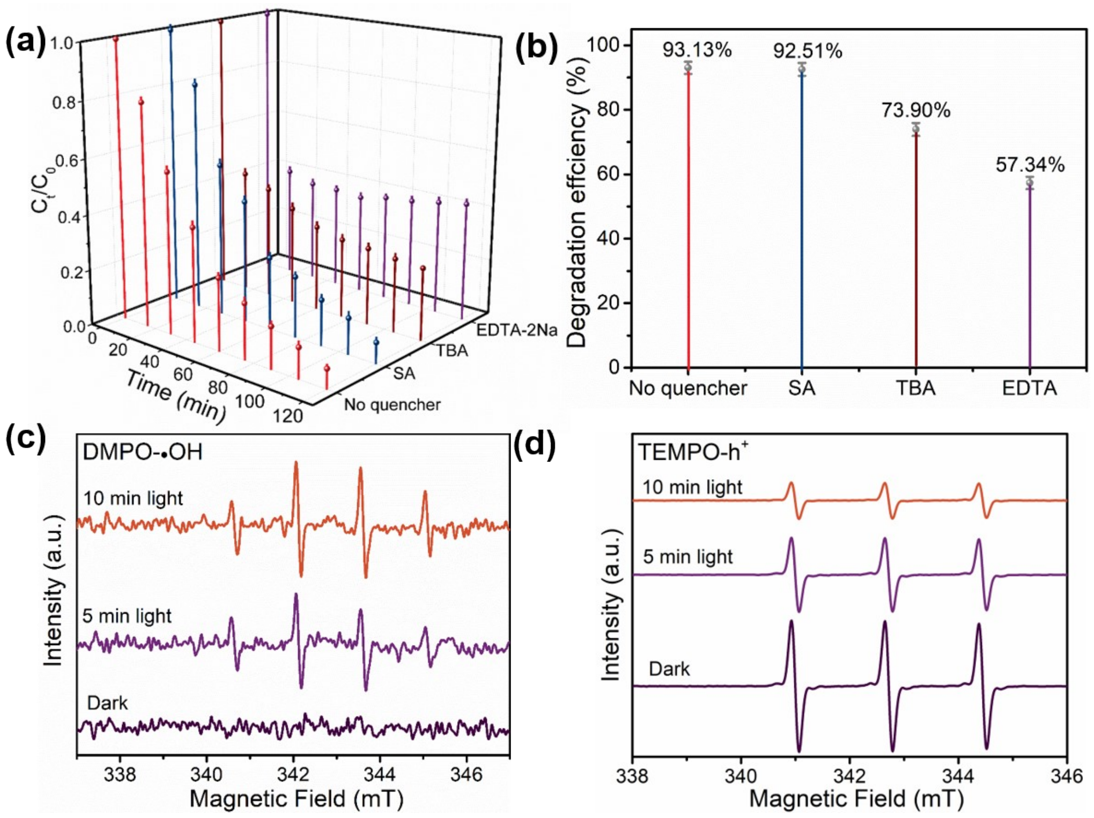

Fig. S6 (a, b) Effects of different radical scavengers on degradation of TC by FTO-α-Fe_2O_3@CeO_2 photoanode; ESR spectra of (c) DMPO-•OH adduct and (d) TEMPO-h$^+$ adduct for FTO-α-Fe_2O_3@CeO_2 photoanode under visible light irradiation (λ > 420 nm).

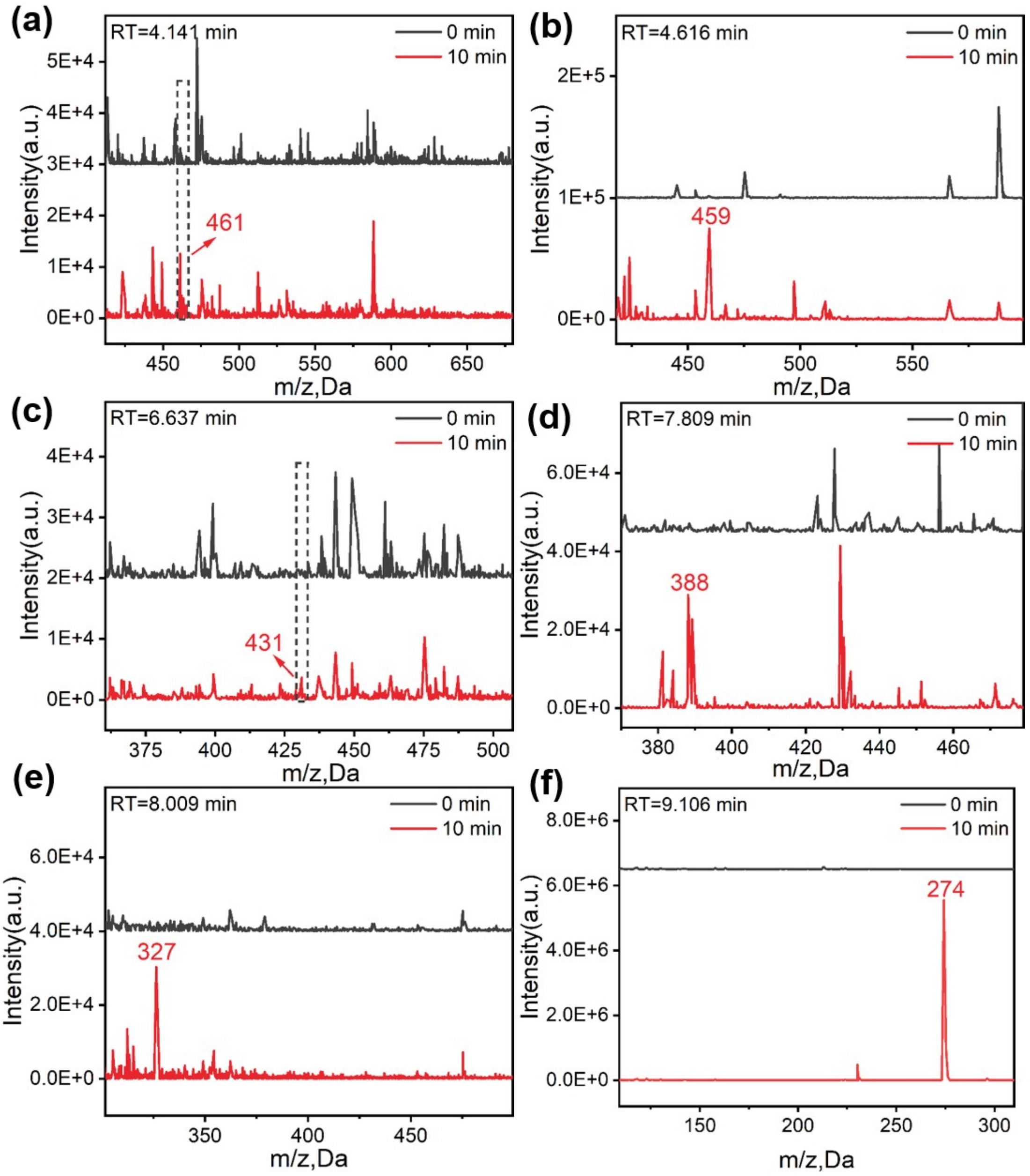

Fig. S7 LC-MS analysis of TC intermediates (P1-P6) by FTO-α-Fe_2O_3@CeO_2 photoanode.

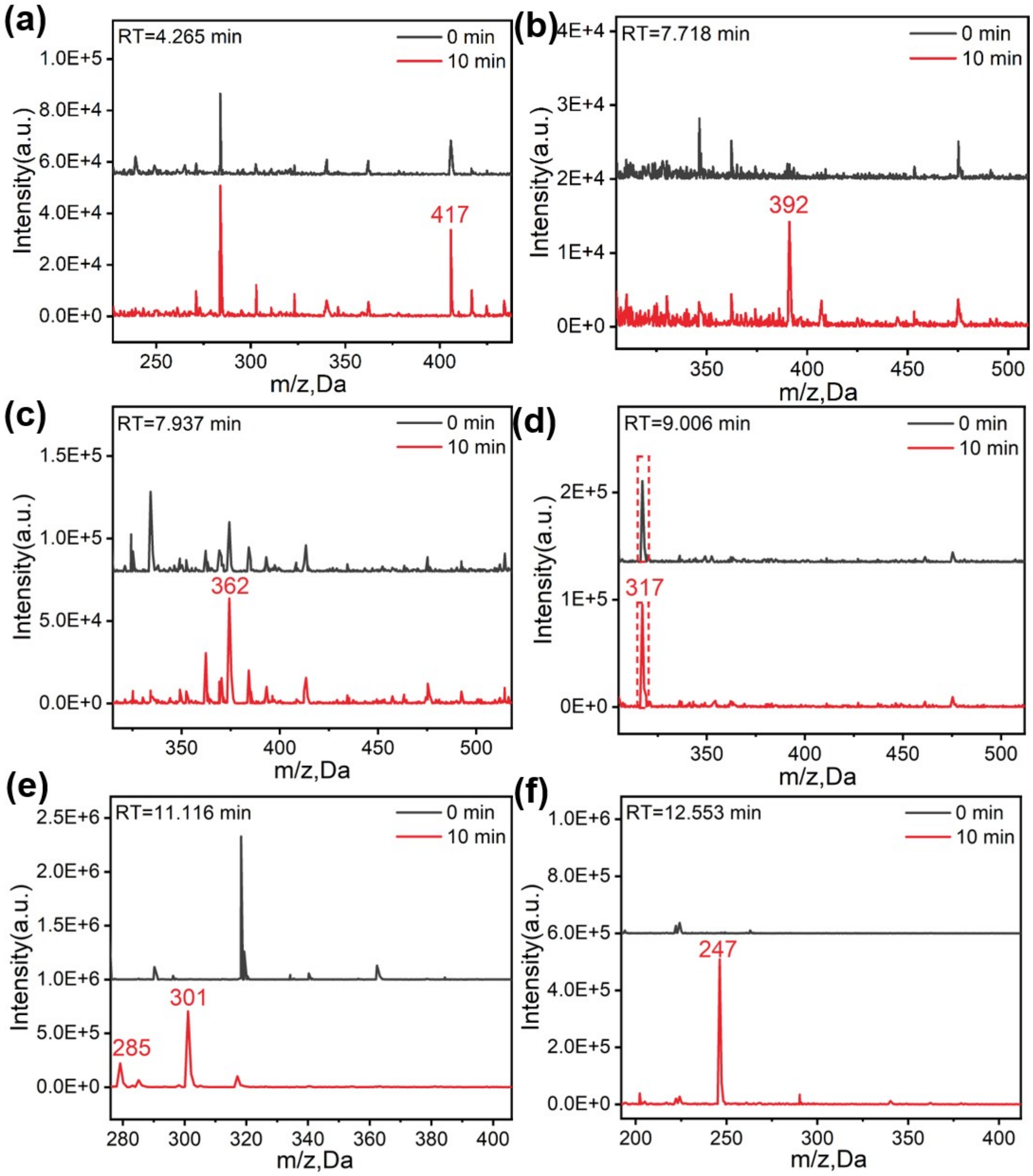

Fig. S8 LC-MS analysis of TC intermediates (P7-P13) by FTO-α-Fe_2O_3@CeO_2 photoanode.

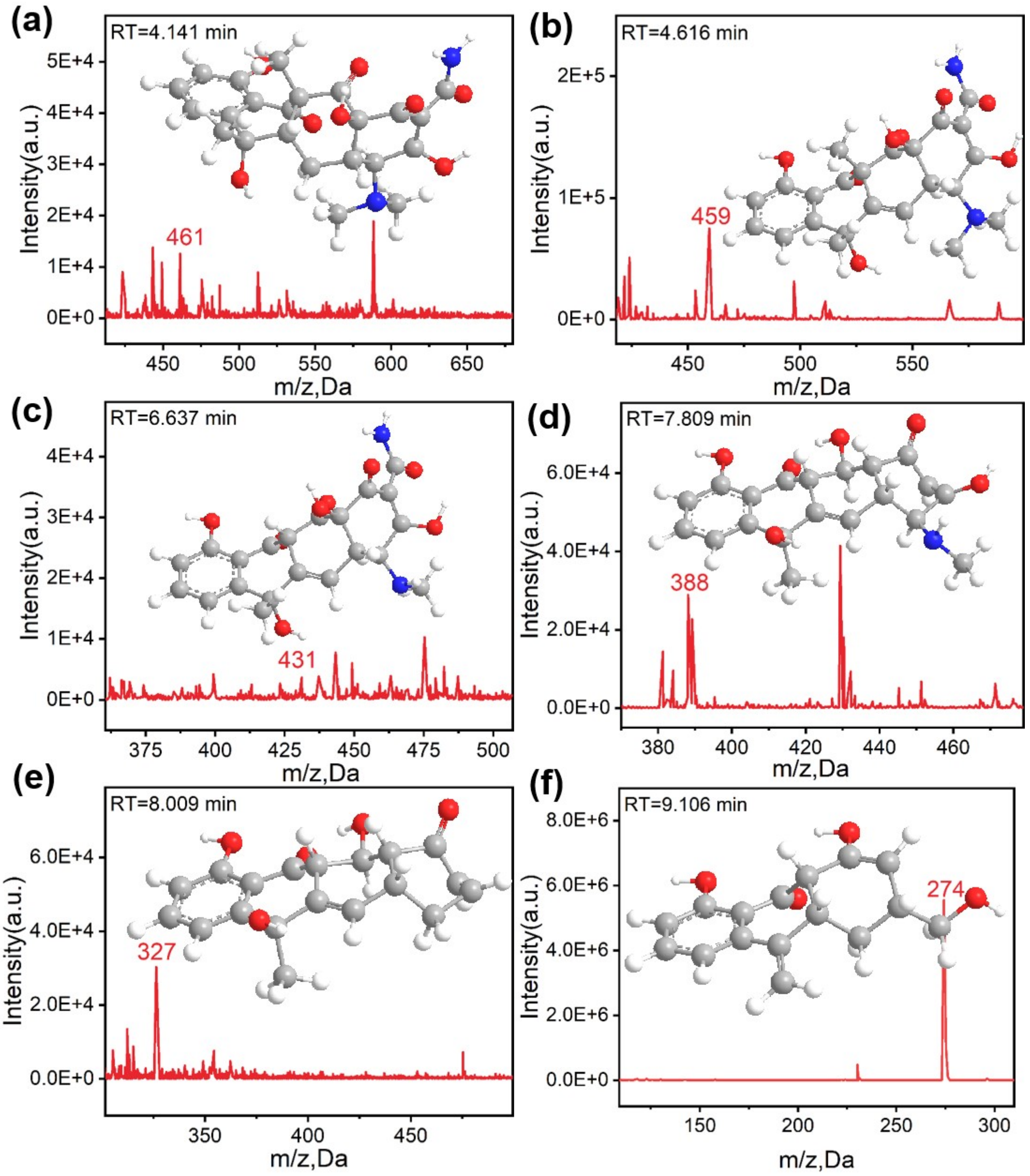

Fig. S9 The intermediates (P1-P6) of TC by FTO-α-Fe_2O_3@CeO_2 photoanode.

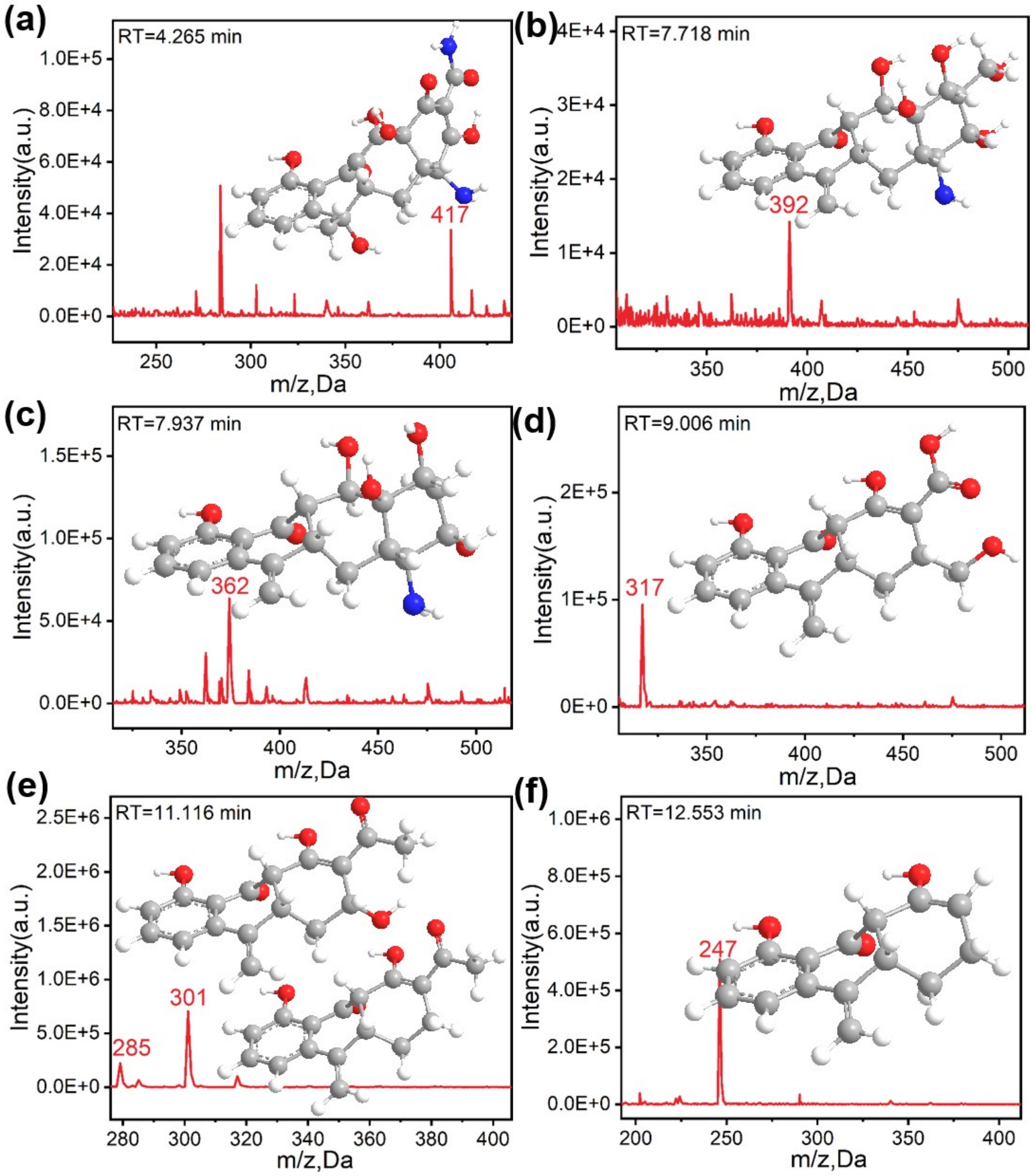

Fig. S10 The intermediates (P7-P13) of TC by FTO-α-Fe_2O_3@CeO_2 photoanode.

Table S1 Degradation of various pollutants by different photoelectrodes.

Photoelectrode	**Current Density**	**k^a/min^{-1}**	**Pollutants**	**Removal efficiency**	**Ref**
TNTAs/P	0.20 mA·cm^{-2}	0.0063	Tylosin 10 mg/L, 100 mL	80.00%-250 min	1
rGO/g-C_3N_4/TNAs	0.28 μA·cm^{-2}	NA^b	Oxytetracycline 20 mg/L, 40 mL	76.59%-60 min	2
PbS/TiO_2	0.08 mA·cm^{-2}	NA	4-chlorobenzoic 5 mg/L, 80 mL	80.37%-420 min	3

TiO_2-NPs/TiO_2-NTs	0.04 mA·cm^{-2}	0.0013	Diclofenac 5 mg/L, 80 mL	62.00%-720 min	4
MI TiO_2, (111) NRs	NA	0.032	Dimethyl phthalate 2 mg/L, 50 mL	88.30%-120 min	5
TNTs-Ag/SnO_2-Sb	0.40 mA·cm^{-2}	NA	α-ethinylestradiol 1.2 mg/L, 100 mL	60.00%-60 min	6
Au/TiO_2-NTs	0.01 mA·cm^{-2}	0.0026	Methyl orange 5 mg/L, 100 mL	56.00%-300 min	7
Ce@Fe-2	NA	0.032	Tetracycline 20 mg/L, 50 mL	88.60%-60 min	8
FTO-α-Fe_2O_3@CeO_2	0.32 mA·cm^{-2}	0.024	Tetracycline 20 mg/L, 100 mL	93.13%-120 min	This study

[a] Rate constant.

[b] NA: Not available.

Table S2 Information and proposed structure of the degradation intermediates from TC

Products	**Molecular Formula**	**m/z**	**Proposed Structure**
TC	$C_{22}H_{25}N_2O_8$	445	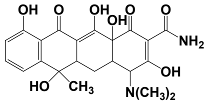
P1	$C_{22}H_{25}N_2O_9$	461	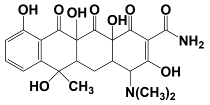
P2	$C_{22}H_{23}N_2O_9$	459	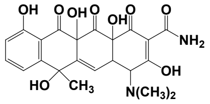
P3	$C_{21}H_{23}N_2O_8$	431	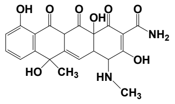
P4	$C_{20}H_{38}NO_6$	388	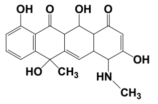
P5	$C_{19}H_{19}O_5$	327	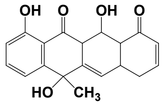
P6	$C_{16}H_{18}O_4$	274	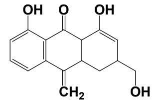
P7	$C_{20}H_{21}N_2O_8$	417	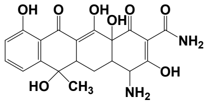

P8	$C_{20}H_{26}NO_7$	392	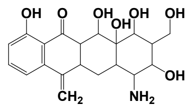
P9	$C_{19}H_{24}NO_6$	362	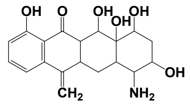
P10	$C_{17}H_{17}O_6$	317	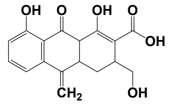
P11	$C_{17}H_{17}O_5$	301	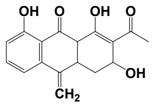
P12	$C_{17}H_{17}O_4$	285	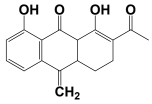
P13	$C_{15}H_{19}O_3$	247	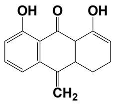

Reference

1. G. Zhang, G. Huang, C. Yang, S. Chen, Y. Xu, S. Zhang, P. Lu, J. Sun, Y. Zhu and D. Yang, Efficient photoelectrocatalytic degradation of tylosin on TiO_2 nanotube arrays with tunable phosphorus dopants, *J. Environ. Chem. Eng*, 2021, **9**, 104742-104749.
2. C. Yu, J. Hou, B. Zhang, S. Liu, X. Pan, H. Song, X. Hou, Q. Yan, C. Zhou, G. Liu, Y. Zhang and Y. Xin, In-situ electrodeposition synthesis of Z-scheme rGO/g-C_3N_4/TNAs photoelectrodes and its degradation mechanism for oxytetracycline in dual-chamber photoelectrocatalytic system, *J. Environ. Manage.*, 2022, **308**, 114615-114625.
3. H. Zhang, Y. Gao, G. Zhu, B. Li, J. Gou and X. Cheng, Synthesis of PbS/TiO_2 nano-tubes photoelectrode and its enhanced visible light driven photocatalytic performance and mechanism for purification of 4-chlorobenzoic acid, *Sep. Purif. Technol.*, 2019, **227**, 115697-115705.
4. X. Cheng, H. Liu, Q. Chen, J. Li and P. Wang, Enhanced photoelectrocatalytic performance for degradation of diclofenac and mechanism with TiO_2 nano-particles decorated TiO_2 nano-tubes arrays photoelectrode, *Electrochim. Acta*, 2013, **108**, 203-210.
5. J. Zhang, B. Tang and G. Zhao, Selective photoelectrocatalytic removal of dimethyl phthalate on high-quality expressed molecular imprints decorated specific facet of single crystalline TiO_2 photoanode, *Appl. Catal., B*, 2020, **279**, 119364-119371.

6. H. He, S. Sun, J. Gao, B. Huang, T. Zhao, H. Deng, X. Wang and X. Pan, Photoelectrocatalytic simultaneous removal of 17alpha-ethinylestradiol and E. coli using the anode of Ag and SnO_2-Sb 3D-loaded TiO_2 nanotube arrays, *J. Hazard. Mater.*, 2020, **398**, 122805-122814.
7. L. Wu, F. Li, Y. Xu, J. W. Zhang, D. Zhang, G. Li and H. Li, Plasmon-induced photoelectrocatalytic activity of Au nanoparticles enhanced TiO_2 nanotube arrays electrodes for environmental remediation, *Appl. Catal., B*, 2015, **164**, 217-224.
8. S. He, C. Yan, X.-Z. Chen, Z. Wang, T. Ouyang, M.-L. Guo and Z.-Q. Liu, Construction of core-shell heterojunction regulating α-Fe_2O_3 layer on CeO_2 nanotube arrays enables highly efficient Z-scheme photoelectrocatalysis, *Appl. Catal., B*, 2020, **276**, 119138-119148.